Available online at www.sciencedirect.com
SCIENCE DIRECT®
Journal of Solid State Chemistry 170 (2003) 374–381
JOURNAL OF SOLID STATE CHEMISTRY
http://elsevier.com/locate/jssc

Extension of the misfit series to the mercury-based cobaltites

D. Pelloquin,* A. Maignan, S. Hébert, C. Michel, and B. Raveau

Laboratoire de cristallographie et Sciences des Materiaux (CRISMAT), UMR CNRS ISMRA 6508, 6 bd Maréchal Juin, 14050 Caen, Cedex, France

Received 25 June 2002; received in revised form 10 October 2002; accepted 20 October 2002

Abstract

The exploration of the Hg–Sr/Ca–Co–O system using EDS and electron microscopy has shown the possibility to incorporate mercury and excess cobalt in the middle rock salt layer of the misfit cobaltite structure, leading to the new series $[Hg_{1-x}Co_xSr_{2-y}Ca_yO_3]^{RS}[CoO_2]_{b1/b2}$ with $0.6 \leqslant x \leqslant 0.90$, $0 \leqslant y \leqslant 2$, and b_1/b_2 ranging from 1.63 to 1.79. These new composite oxides, built up from $[CoO_2]_\infty$ layers of the CdI_2-type stacked with triple $[Hg_{1-x}Co_xSr_{2-y}Ca_yO_3]$. rock salt layers are remarkable by their large thermopower S values similarly to the thallium and lead misfit cobaltites. More importantly, the S value is sensitive to the composition of the triple rock salt layer, increasing as the calcium content increases, so that an enhancement of the figure of merit of the pure calcium compound is expected.

1. Introduction

Oxides represent a huge source for the generation of new properties as shown with the discovery of superconductivity at high temperature in cuprates and more recently of colossal magnetoresistance in manganites. In this respect cobalt-based oxides are also promising candidates as thermoelectric materials as shown by the report of a large thermopower value in the metallic oxide $NaCo_2O_4$ [1]. More recently, very similar thermoelectric properties were found in the metallic misfit cobaltite $Ca_3Co_4O_9$ [2–4]. The latter, stable in air at high temperature, has been used in an all-oxide thermoelectric power generator operating at 773°C [5], demonstrating the potentiality of metal oxides as thermoelectric materials for high-temperature applications. The $Ca_3Co_4O_9$ compound, also formulated $[CoCa_2O_3]^{RS}[CoO_2]_{1.62}$ to show the misfit character of its structure, can be described as a 2D triangular Co sheets of the CdI_2-type containing edge-shared CoO_6 octahedra, separated by triple rock salt-type $[CoCa_2O_3]_\infty$ layers [3,4,6]. The large thermopower Seebeck (S) values of $NaCo_2O_4$ and $Ca_3Co_4O_9$, ranging from $S = 100$ to $120\,\mu V\,K^{-1}$, might be ascribed to the low spin state configurations of trivalent and tetravalent cobalt cations that form the 2D triangular lattice [7]. Such results have intensified the research in cobaltites in order to improve their thermoelectric properties and realize some devices operating at $T \gg 300$ K. In parallel to the compounds derived from $Ca_3Co_4O_9$, other systems associated with the substitution of calcium for strontium have been investigated and some misfit stackings have been observed in the Tl–Sr/Ca–Co–O [8,9] and Pb–Sr/Ca–Co–O [10,11] systems. In those systems, the influence of the composition of the rock salt-type layers on the thermopower is emphasized by the significant enhancement of the RT thermopower with the highest value of $165\,\mu V\,K^{-1}$ in $[Pb_{0.4}Co_{0.6}Ca_2O_3]^{RS}[CoO_2]_{1.61}$ [11] and by the regular increase of the S value, from 120 to $165\,\mu V\,K^{-1}$ as the calcium content increases, observed in the lead-based misfit cobaltites.

Considering the similarity of the [AO] layers belonging to the rock salt-type block, in the 2D structures of both cuprate and misfit cobaltite, it turns out that mercury is also a potential candidate to build new cobaltites by introducing Hg at the level of rock salt-type layers as in superconducting cuprates [12]. We report herein on a new series of misfit cobaltites with nominal compositions $Hg_{1-x}Sr_{2-y}Ca_yCo_{1.8+x}$, with $0.60 \leqslant x \leqslant 0.90$ and $0 \leqslant y \leqslant 2$. From electron microscopy and EDS observations we determine the actual formula and structural parameters of these oxides. We show that these misfit oxides exhibit high thermopower values but, more importantly, that the substitution of calcium for strontium increases the thermopower while resistivity

*Corresponding author. Fax: 02-31-96-16-00.
E-mail address: pelloquin@ismra.fr (D. Pelloquin).

0022-4596/03/$ - see front matter © 2002 Elsevier Science (USA). All rights reserved.
doi:10.1016/S0022-4596(02)00129-9

only slightly increases, suggesting an enhancement of the figure of merit for the pure calcium phase compared to strontium.

2. Experimental

The synthesis of polycrystalline samples is derived from the method used in the case of Pb-based misfit cobaltites [10,11]. Stoichiometric amounts of oxides and peroxides, HgO, SrO_2, CaO and Co_3O_4 are weighted according to the nominal cation composition $Hg_{1+y}Sr_{2-y}Ca_yCo_{2.4}$ with y varying from 0 to 2. A large oxygen partial pressure is necessary to obtain nearly pure samples. So an excess of mercury oxide with regard to the generic misfit formula $[(Hg_{1-x}Co_x)(Sr_{2-y}Ca_y)O_3]^{RS}[CoO_2]_{1.8}$ is intentionally introduced to keep a nominal oxygen stoichiometry close to 8. Then the oxides are mixed and pressed in the form of bars. The samples are placed in silica tubes sealed under vacuum with approximately 0.8 g of sample for a volume of 3 cm^3 in the tube. The samples are heated up to 900°C with a heating rate of 150°C h^{-1}, maintained at this temperature for 12 h and cooled down to room temperature at the same cooling rate. Black ceramic bars are obtained and some mercury metal droplets are systematically observed in the tubes.

The electron diffraction (ED) studies are carried out using a JEOL 200CX microscope fitted with an eucentric goniometer ($\pm 60°$) while the high-resolution electron microscopy (HREM) images are recorded with a TOPCON 02B operating at 200 kV and having a point resolution of 1.8 Å (Cs = 0.4 mm). Both microscopes are equipped with KEVEX EDS analyzers. The interpretation of experimental images is performed from HREM image simulations calculated with the Mac-Tempas multislice software. The actual cation ratio is determined from energy dispersive spectroscopy (EDS) analyses carried out on numerous crystallites.

X-ray diffraction data are collected at room temperature using a XpertPro Philips vertical diffractometer working with the Cu$K\alpha$ radiation and equipped with a secondary graphite monochromator. Data collection is carried out by continuous scanning (step = 0.02° (2θ), preset = 10 s) over an angular range $10° \leqslant 2\theta \leqslant 80°$. Lattice constants and structural calculations were refined by the Rietveld method using the computer program JANA2000 [13].

The magnetic properties are studied using a SQUID magnetometer (ac and dc; 0–5T; 1.8–400 K). Resistance data as a function of temperature (1.8–400 K) or magnetic field (0–7 T) are collected with a quantum design physical properties measurement system (PPMS) by the four-probe technique. Current and voltage indium contacts are ultrasonically deposited on the sintered bars (typically $2 \times 2 \times 10\,mm^3$). A steady-state method is used to measure the Seebeck effect (S) in the PPMS with high-temperature limit fixed at 320 K by the calibration range of the temperature sensors.

3. Results and discussion

3.1. Composition and structural characteristics

Due to the thermal decomposition of HgO and mercury volatilization, the actual composition of the different samples is systematically different from the nominal one, and depends on the synthesis conditions, especially on the partial oxygen pressure and the temperature. For these reasons, a systematic cationic analysis by EDS, coupled with an electron diffraction (ED) characterization is absolutely necessary for each sample and must be carried out each time on numerous microcrystals (i.e. about 20 for each sample) in order to test the homogeneity. From these observations we have determined that the misfit-type structure is obtained as a nearly pure phase (minor phases, such as $SrHgO_2$ or HgO, have also been detected) in the powder samples for the global compositions $Hg_{1-x}Sr_{2-y}Ca_yCo_{1.8+x}$ with x ranging from 0.6 to 0.9 as y increases from $y = 0$ to 2. The corresponding actual cationic compositions obtained by EDS for four significant samples—pure strontium, pure calcium, and two intermediate compositions—are given in Table 1. They show that the actual mercury content is much smaller than the nominal one, as expected, but the content of other cations (Co, Ca, Sr) is preserved.

The powder X-ray diffraction data of these oxides confirms the analogy of those samples with the Tl–Sr/Ca–Co–O and Pb–Sr/Ca–Co–O misfit cobaltites [8–11]. The lattice parameters of the four above compositions are listed in Table 1. They have been obtained from profile refinements performed in a 4D formalism, taking into account the composite character of the misfit structure. The original structural model, derived from the homologous misfit cobaltites $[CoCa_2O_3]^{RS}[CoO_2]_{b1/b2=1.62}$ [3,4,6] and $[(Pb_{0.7}Co_{0.3})Sr_2O_3]^{RS}[CoO_2]_{b1/b2=1.8}$ [10] is indeed composed of two subcells—the first one S_1 related to triple [AO] rock salt layers and the second one S_2 related to a CdI_2-type structure. These two subcells coexist through a common monoclinic plane (a, c, β) and the $C2/m$ $(1d0)s0$ super space group whereas the misfit component is ascribed to the ratio b_1/b_2. A view of this structural model is shown in Fig. 1.

The evolution of the cell parameters (Fig. 2) evidences a continuous decrease of the b_1/b_2 ratio as calcium substitutes for strontium while the mercury content and the c stacking parameter decrease. This evolution corroborates the analysis of ED[001] oriented patterns in which a decrease of the b_1/b_2 ratio can also be observed and is in agreement with the isovalent

Table 1
$Hg_{1-x}Sr_{2-y}Ca_yCo_{b1/b2+x}$

Nominal compositions	Cationic compositions (EDS)	x	y	a (Å)	b_1 (Å)	c (Å)	β (deg)	b_1/b_2
$Hg_{0.6}Sr_2Co_{2.4}$	$Hg_{0.39}Sr_2Co_{2.37}$	0.61	0	4.936(1)	5.019(1)	11.425(2)	97.93(1)	1.791(1)
$Hg_{1.6}SrCaCo_{2.3}$	$Hg_{0.37}Sr_{0.93}Ca_{1.07}Co_{2.67}$	0.63	1.07	4.882(3)	4.791(2)	11.183(7)	97.94(4)	1.699(3)
$Hg_{2.1}Sr_{0.5}Ca_{1.5}Co_{2.3}$	$Hg_{0.29}Sr_{0.6}Ca_{1.4}Co_{2.42}$	0.71	1.4	4.873(2)	4.686(2)	11.026(6)	98.07(3)	1.670(2)
$Hg_{2.6}Ca_2Co_{2.3}$	$Hg_{0.09}Ca_2Co_{2.51}$	0.91	2	4.842(1)	4.595(1)	10.904(2)	98.08(3)	1.632(1)
Ref. [3]	$Ca_3Co_4 \equiv Ca_2Co_{2.67}$	1	2	4.837(1)	4.556(1)	10.833(1)	98.06(1)	1.616(1)

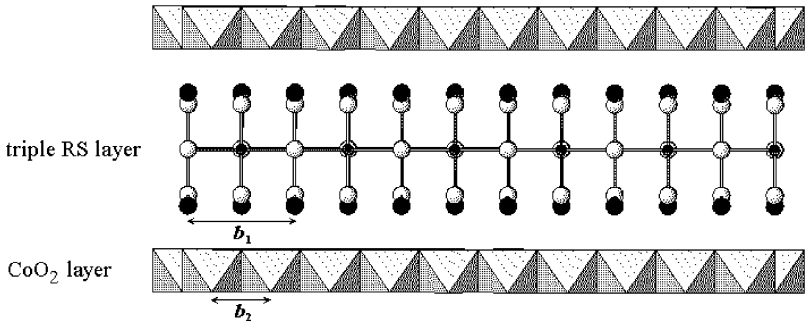

Fig. 1. Structural model of the $[AO]_3^{RS}[CoO_2]_{b1/b2}$ misfit cobaltite.

substitution of strontium for smaller alkaline earth. Note that the same behavior has been observed in the Tl–Sr/Ca–Co–O [8] and Pb–Sr/Ca–Co–O [10,11] misfit cobaltites with the decrease of the thallium or lead content as calcium is introduced. In the case of lead-based misfit cobaltites the proposed model, namely $[Pb_{0.7-x}Co_{0.3+x}(Sr,Ca)_2O_3]^{RS}[CoO_2]_{b1/b2}$, includes cobalt species in the S_1 rock salt-type subcell. Moreover the lead and cobalt contents in the latter subcell seem to be related. This is shown in Table 2 where the analytical results obtained for $Tl_{0.8-x}(Sr,Ca)_2Co_2O_{6+\delta}$ [8] and $Hg_{0.4-x}(Sr,Ca)_2Co_{2.4}O_{6+\delta}$ misfit series are also reported. Taking into account the global cationic compositions deduced from the EDS analyses and considering the same model for the three studied systems, the experimental b_1/b_2 ratio indeed tends to decrease as cobalt species replaces thallium or lead or mercury. Nevertheless, no general trend can be proposed between the evolution of this misfit b_1/b_2 ratio, the lattice parameters and the excess of cobalt sitting in S_1 subcell. This can be illustrated by the structural behavior reported for the misfit $Tl_\alpha Sr_2Co_{2.1}O_{6+\delta}$ cobaltites, which formula can be rewritten as $[Tl_xCo_ySr_{3-x-y}O_3]^{RS}[CoO_2]_{b1/b2}$ [9]. For the latter, the Co content y decreases from 0.33 to 0.03 as the Tl content x increases from 0.76 to 1.18. In contrast to the behavior observed in the case of Hg-series, the c-axis increases from 11.6 to 11.7 Å as the b_1/b_2 ratio decreases from 1.8 to 1.76. Thus the various mismatches between the two sublattices, S_1 and S_2, in these misfit cobaltites cannot be simply ascribed to the content of either post-transition or cobalt species inside the rock salt-type sublattice. By considering the synthesis conditions (oxygen pressure in the tube), it is also unlikely that an oxygen defiency is responsible for this structural evolution. It turns out that the different mismatch values, characterized by the b_1/b_2 ratios, are governed by the whole cationic composition and average steric environment of the rock salt-type sublattice. This feature is perfectly illustrated by the comparison of the $[Pb_{0.4}Co_{0.6}Ca_2O_3]^{RS}[CoO_2]_{1.61}$ and $[Hg_{0.39}Co_{0.57}Sr_2O_3]^{RS}[CoO_2]_{1.79}$ oxides. They exhibit some different experimental b_1/b_2 ratios whereas the same excess of cobalt sitting in rock salt subcell can be deduced from EDS analyses (Table 2). It is clearly the very different ionic radii of Sr^{2+} and Ca^{2+} that makes the variation of the b_1/b_2 ratio.

3.2. HREM investigations

In order to understand the cationic distribution inside the rock salt layers, and especially to evidence the possible location of mercury and cobalt excess in the middle layer, a HREM study has been carried out in the pure strontium $[Hg_{0.4}Co_{0.6}Sr_2O_3]^{RS}[CoO_2]_{1.8}$ misfit cobaltite.

As previously reported in $[CoCa_2O_3]^{RS}[CoO_2]_{1.62}$ [3,6] and the lead-based misfit cobaltites [10,11], the experimental [100] or [010] oriented images clearly show a periodic stacking of four specific layers along the c-axis. The analysis of the contrasts shows a stacking of a block of three similar rows of dots interleaved by a single row of more and less diffuse spots. The HREM images, shown in Fig. 3 illustrate these observations which allow to correlate the contrasts to a regular stacking of triple rock salt-type layers with single $[CoO_2]$ layers.

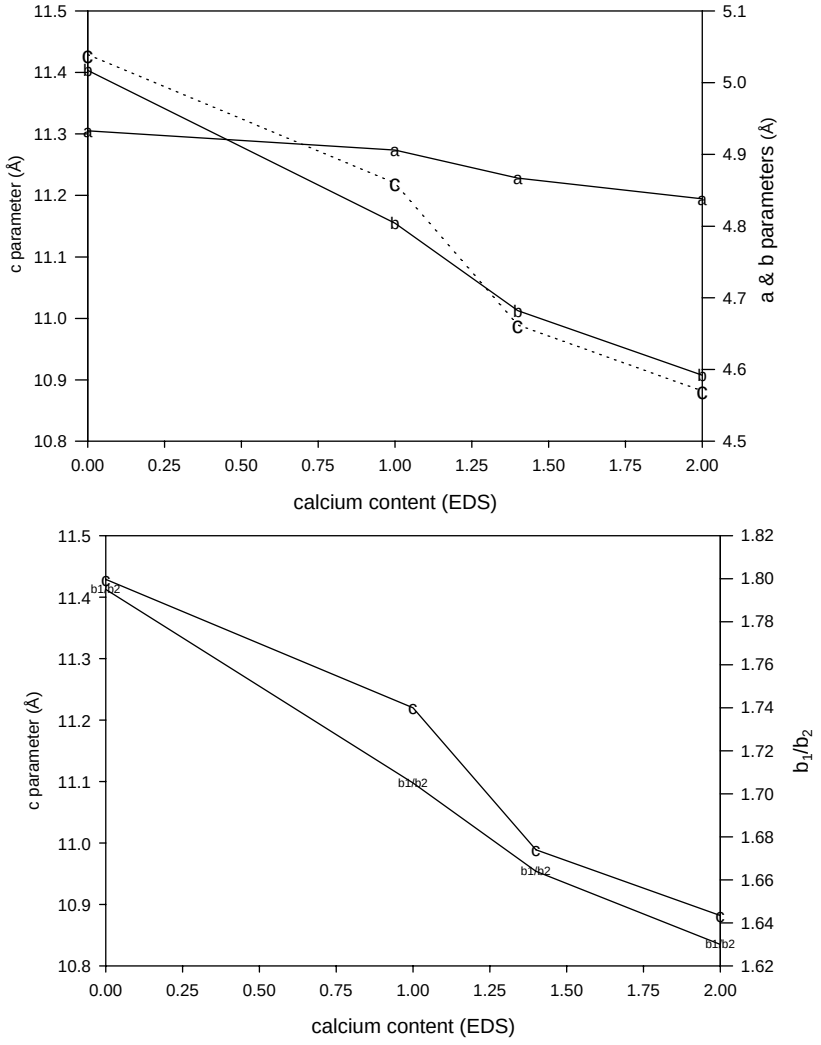

Fig. 2. Cell parameters evolution of the solid solution $Hg_{1-x}Sr_{2-y}Ca_yCo_{b1/b2+x}$.

Table 2

	Cationic compositions (EDS)	b_1/b_2	$\times M$ (Pb,Tl,Hg)	y Co	$[AO]_3^{RS}[CoO_2]_{b1/b2}$
Refs. [10,11]	$Pb_{0.7}Sr_2Co_{2.1}$	1.79	0.69	0.31	$[Pb_{0.69}Co_{0.31}Sr_2O_3]^{RS}[CoO_2]_{1.79}$
	$Pb_{0.63}(Sr_{1.47}Ca_{0.53})Co_{2.37}$	1.75	0.6	0.50	$[Pb_{0.6}Co_{0.5}Sr_{1.4}Ca_{0.5}O_3]^{RS}[CoO_2]_{1.75}$
	$Pb_{0.74}(Sr_{1.05}Ca_{0.95})Co_{2.22}$	1.71	0.7	0.40	$[Pb_{0.7}Co_{0.4}SrCa_{0.9}O_3]^{RS}[CoO_2]_{1.71}$
	$Pb_{0.66}(Sr_{0.67}Ca_{1.33})Co_{2.52}$	1.67	0.6	0.60	$[Pb_{0.6}Co_{0.6}Sr_{0.6}Ca_{1.2}O_3]^{RS}[CoO_2]_{1.67}$
	$Pb_{0.4}Ca_2Co_{2.2}$	1.61	0.4	0.59	$[Pb_{0.4}Co_{0.6}Ca_2O_3]^{RS}[CoO_2]_{1.61}$
This work	$Hg_{0.39}Sr_2Co_{2.37}$	1.79	0.39	0.57	$[Hg_{0.39}Co_{0.57}Sr_2O_3]^{RS}[CoO_2]_{1.79}$
	$Hg_{0.37}Sr_{0.93}Ca_{1.07}Co_{2.67}$	1.70	0.35	0.77	$[Hg_{0.35}Co_{0.77}Sr_{0.87}Ca_{0.99}O_3]^{RS}[CoO_2]_{1.70}$
	$Hg_{0.29}Sr_{0.6}Ca_{1.4}Co_{2.42}$	1.67	0.29	0.72	$[Hg_{0.29}Co_{0.72}Sr_{0.59}Ca_{1.38}O_3]^{RS}[CoO_2]_{1.66}$
	$Hg_{0.09}Ca_2Co_{2.51}$	1.63	0.09	0.88	$[Hg_{0.09}Co_{0.88}Ca_{2.03}O_3]^{RS}[CoO_2]_{1.63}$
Ref. [8]	$Tl_{0.82}Sr_2Co_2$	1.79	0.81	0.20	$[Tl_{0.81}Co_{0.2}Sr_{1.99}O_3]^{RS}[CoO_2]_{1.79}$
	$Tl_{0.69}(Sr_{1.45}Ca_{0.52})Co_{2.09}$	1.76	0.69	0.34	$[Tl_{0.69}Co_{0.34}Sr_{1.45}Ca_{0.52}O_3]^{RS}[CoO_2]_{1.76}$
	$Tl_{0.63}(Sr_{0.99}Ca_{0.99})Co_{2.1}$	1.72	0.62	0.37	$[Tl_{0.62}Co_{0.37}SrCaO_3]^{RS}[CoO_2]_{1.72}$
	$Tl_{0.50}(Sr_{0.49}Ca_{1.50})Co_{2.19}$	1.69	0.5	0.50	$[Tl_{0.5}Co_{0.5}Sr_{0.5}Ca_{1.5}O_3]^{RS}[CoO_2]_{1.69}$
	$Tl_{0.38}Ca_2Co_{2.25}$	1.64	0.38	0.61	$[Tl_{0.38}Co_{0.61}Ca_2O_3]^{RS}[CoO_2]_{1.64}$
Ref. [9]	$Tl_{0.76}Sr_2Co_{2.12}$	1.79	0.76	0.33	$[Tl_{0.76}Co_{0.33}Sr_2O_3]^{RS}[CoO_2]_{1.79}$
	$Tl_{1.08}Sr_2Co_{2.02}$	1.78	1.01	0.11	$[Tl_{1.01}Co_{0.11}Sr_{1.88}O_3]^{RS}[CoO_2]_{1.78}$
	$Tl_{1.32}Sr_2Co_{2.0}$	1.76	1.18	0.03	$[Tl_{1.18}Co_{0.03}Sr_{1.78}O_3]^{RS}[CoO_2]_{1.76}$
Refs. [3,4,6]	$Ca_3Co_4 \equiv Ca_2Co_{2.67}$	1.62	–	1.0	$[CoCa_2O_3]^{RS}[CoO_2]_{1.62}$

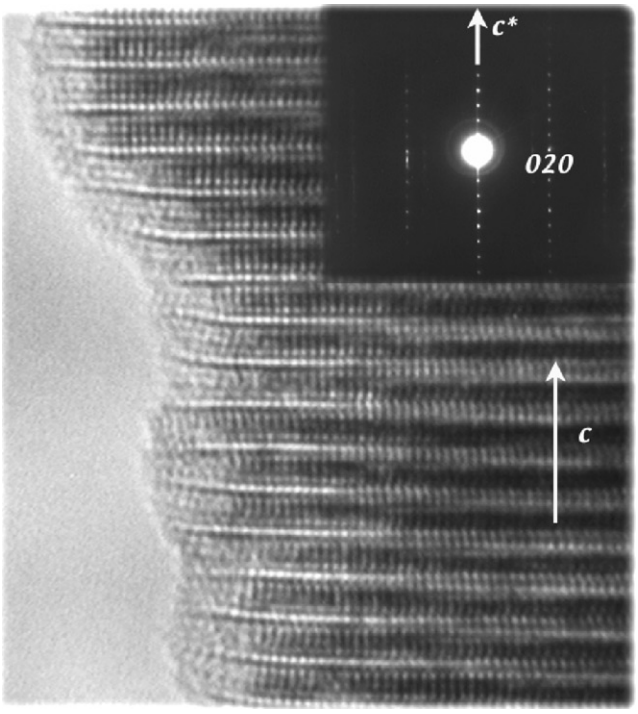

Fig. 3. Experimental [1 0 0] oriented HREM images of $[Hg_{0.4}Co_{0.6}Sr_2O_3]^{RS}[CoO_2]_{1.79}$ misfit cobaltite recorded with a defocus value close to 50 Å. Corresponding electron diffraction pattern is inserted.

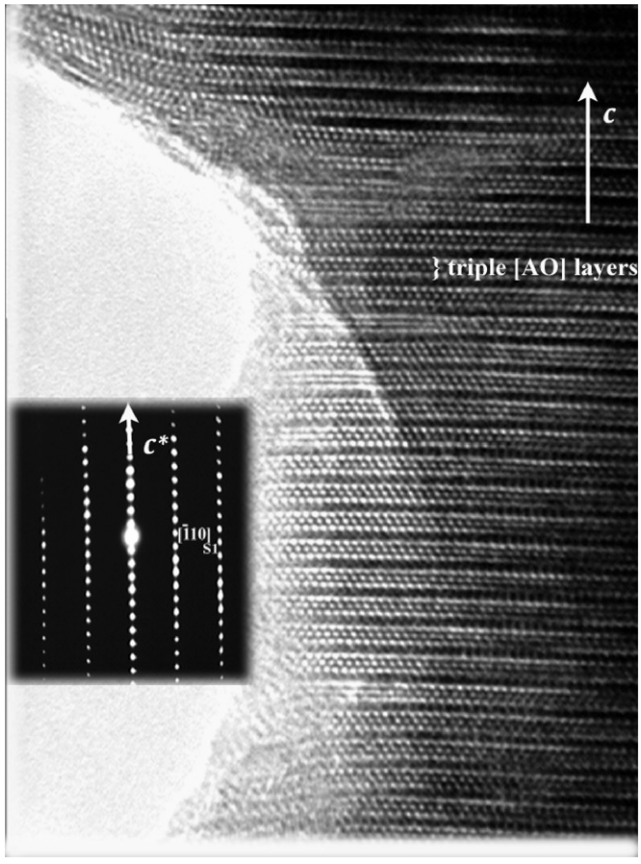

Fig. 4. Experimental $[1\,1\,0]_{s1}$ oriented HREM image of $[Hg_{0.4}Co_{0.6}Sr_2O_3]^{RS}[CoO_2]_{1.79}$ misfit cobaltite. Corresponding electron diffraction pattern is inserted.

The rock salt nature of the $[Hg_{0.4}Co_{0.6}Sr_2O_3]_\infty$ layers is also confirmed by the $[110]_{s1}$ HREM image (Fig. 4) in which the defocus value, close to −500 Å, images the zones of high electron densities as bright dots. One indeed observes triple rows of staggered bright dots spaced by 3.6 Å along $[1\bar{1}0]_{s1}$, corresponding to the triple rock salt layers, separated along $\vec{c}$ by single rows of diffuse gray dots corresponding to the $[CoO_2]_\infty$ layers. From the HREM observations and experimental defocus values studied, the image contrasts of each rock salt-type layers are rather homogeneous suggesting a random distribution of cations within these layers. This great ability of rock salt layers to accommodate simultaneously numerous cations is not particular to the misfit cobaltites. It has indeed been observed in the cuprates and cobaltites forming intergrowths between the rock salt and the perovskite structures with a random or ordered cation distribution as shown in the 1201-type cobaltite (Tl,Sr)-1201 [14] or ordered (Bi,Sr)-1201 [15]. However, the comparison of contrasts ascribed to triple rock salt-type layers (Figs. 3 and 4) versus the defocus value allows to foresee a preferential occupation of the middle rock salt layer also suggested by the different cationic compositions, especially the sum $x+y$ (Table 2). To confirm this structural feature, the same $[110]_{s1}$ oriented crystal (Fig. 4) has been recorded with different focus values. These successive HREM images are shown in Fig. 5. The image contrasts are interpreted by comparing these experimental images with those previously reported in mixed layered cobalt-based oxides and those simulated from atomic positions and occupancy sites refined in a 3D commensurate Cm supercell ($b_1/b_2 = 1.8 = 9/5$) [3,6]. This work allows again to observe without ambiguity the triple rock salt-type layers regularly spaced by a $[CoO_2]$ layer. Although the strong lamellar character of these materials disturbs the comparison between the three [AO] layers, for small areas the middle [AO] layer exhibits a different contrast from the two others. This observation, illustrated by the enlarged Fig. 5a in which cationic rows are imaged as bright dots (the defocus value is estimated close to 50 Å), suggests a preferential filling of this layer by mercury and cobalt species. The structural refinements considering such a cation distribution, i.e. close to 40% Hg and 60% Co in the middle layer, lead to a reliability factor $R_{intensity}$ close to 0.09. This distribution is compatible with the mercury (II) which adopts usually a dumb-bell coordination (two short apical distances close to 2 Å) like observed, from neutron diffraction data, in the homologous mixed rock salt-type $[(Hg_{0.5}M_{0.5})O]$ (M = Cr) layers of the superconducting cuprates [12]. Next, simulated images have

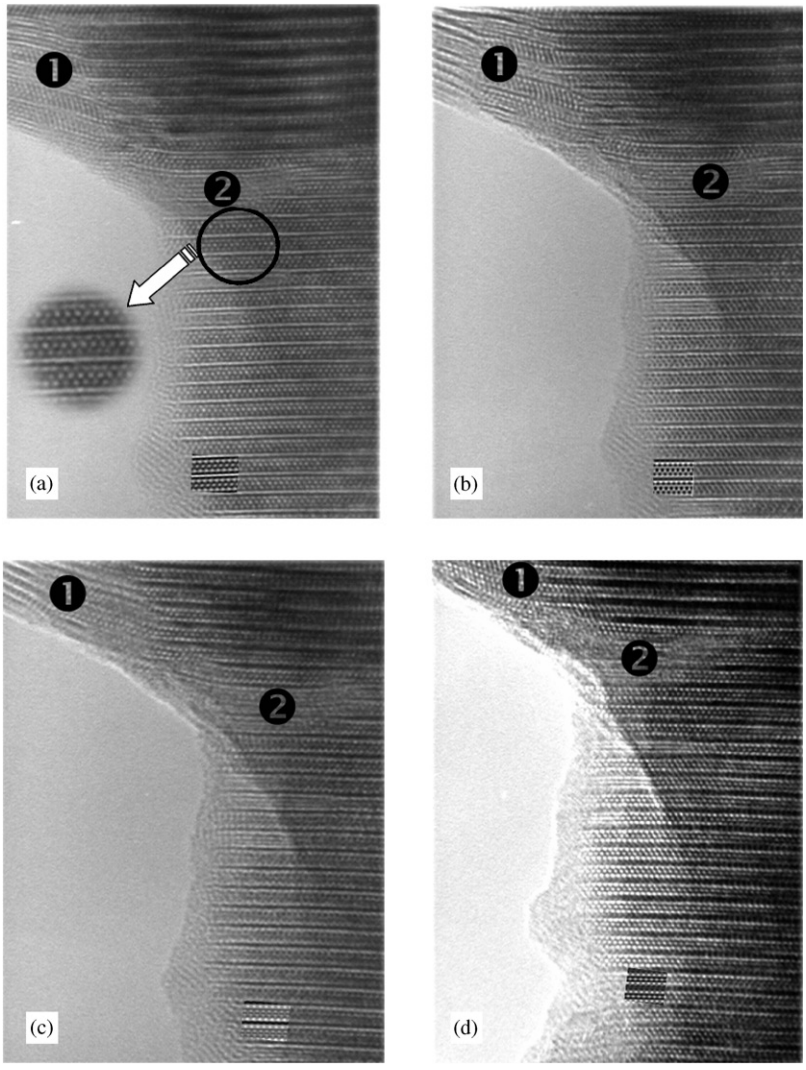

Fig. 5. Focus values series recorded on the same $[1\,1\,0]_{s1}$ oriented zone: $\Delta f = 50$ Å (a), -250 Å (b), -350 Å (c), and -500 Å (d), respectively. The corresponding simulated contrasts calculated with a thickness close to 36 Å are inserted.

been calculated from these positions and occupations considering a crystal thickness of 36 Å with a defocus value ranging from 100 to -900 Å. The calculated contrasts inserted in Fig. 5 fit well our different experimental HREM images and validate the structural model.

In contrast to the HREM images reported in the other layered cobalt-based oxides, such as (Bi,Sr)-1201-type cobaltites [15], few ordering mechanisms or extended stacking faults have been detected. However, some tiny disordered zones (about 200 Å^2) are locally observed (labelled 1 and 2 in Fig. 5). From the Fourier calculations (FFT) of these zones, most of the resulting patterns appear slightly disoriented (label 1) in agreement with the strong lamellar character of these layered structures. In places these defects can be ascribed to a stacking fault (label 2).

3.3. Transport properties

The resistivity curves of the four investigated samples are displayed in Fig. 6. The Ca free sample (curve a) exhibits a metallic behavior for $T > 30$ K and the room temperature resistivity is small, close to 50 mΩ cm, as for the Tl family or Pb family of misfits. At low temperature, ρ increases as T decreases but the increase is very small as $\rho_{5\,K}$ is only 30 mΩ cm. The influence of Ca is first to increase ρ in the whole range of temperature: for example, $\rho_{300\,K}$ is close to 100 mΩ cm for $Hg_{0.29}Sr_{0.6}Ca_{1.4}Co_{2.42}$ (curve c) and a strong localization is observed in this sample for $T < 140$ K, $\rho_{5\,K}$ reaching 40 Ω cm. When Sr is completely substituted by Ca, the resistivity (curve d) decreases again in the whole temperature range, with a smaller localized behavior below 100 K as $\rho_{5\,K}$ increases only to

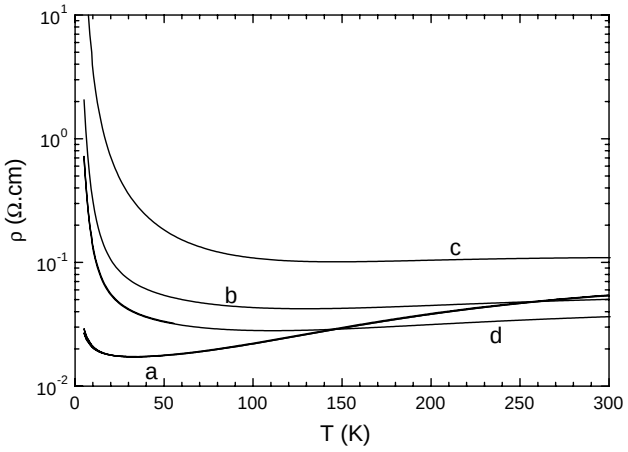

Fig. 6. T dependence of the resistivity (ρ) of the Hg/Sr/Ca/Co/O misfit cobaltites: (a) $[Hg_{0.39}Co_{0.57}Sr_2O_3]^{RS}[CoO_2]_{1.79}$, (b) $[Hg_{0.29}Co_{0.72}Sr_{0.59}Ca_{1.38}O_3]^{RS}[CoO_2]_{1.66}$, (c) $[Hg_{0.29}Co_{0.72}Sr_{0.59}Ca_{1.38}O_3]^{RS}[CoO_2]_{1.66}$ and (d) $[Hg_{0.09}Co_{0.88}Ca_{2.03}O_3]^{RS}[CoO_2]_{1.63}$.

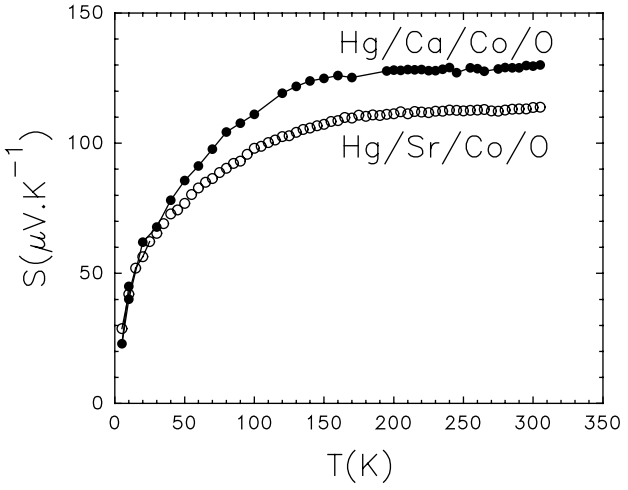

Fig. 7. T dependence of the thermopower (Seebeck S) for the pure Sr (Hg/Sr/Co/O) and pure Ca (Hg/Ca/Co/O) misfit cobaltites.

0.7 Ω cm, and with the smallest room temperature resistivity of the whole family $\rho_{300\,K} = 40$ mΩ cm for $Hg_{0.09}Ca_2Co_{2.51}$.

The thermopower S of the end members ($[Hg_{0.39}Co_{0.57}Sr_2O_3]^{RS}[CoO_2]_{1.79}$ and $[Hg_{0.09}Co_{0.88}Ca_{2.03}O_3]^{RS}[CoO_2]_{1.63}$ oxides) is shown in Fig. 7. The room temperature S value increases from $+115\,\mu V\,K^{-1}$ for the Ca free sample to $+130\,\mu V\,K^{-1}$ for the Sr free sample.

The Ca substitution is thus an effective method to improve the thermopower of these Hg-based misfits. Similar results were obtained in the Pb family [11]: S can be increased from $+120\,\mu V\,K^{-1}$ for $[Pb_{0.7}Co_{0.3}Sr_2O_3][CoO_2]_{1.79}$ to $+165\,\mu V\,K^{-1}$ for $[Pb_{0.4}Co_{0.6}Ca_2O_3][CoO_2]_{1.61}$. For this family, it has been shown that the Ca substitution is not the only factor responsible for the improvement of S, and that the presence of Pb in the RS-type layers was necessary to reach large S value. In the Hg family, the substitution of Sr by Ca is also not the only parameter which governs S and ρ. Indeed, as Ca is introduced, the Hg content simultaneously decreases in the RS-type layer and is drastically reduced to 0.09 for the Sr free sample. This can explain the only moderate impact on the S value and the non-monotonic evolution of ρ with Ca content: ρ first continuously increases as the Sr content decreases (curves a–c in Fig. 6) with an almost constant Hg content, then ρ decreases again for the Sr free compound (curve d in Fig. 6).

This suggests that the Ca substitution is beneficial for the power factor S^2/ρ: first S increases when going from the Sr sample to the Ca sample, and second the detrimental increase of ρ when Ca is partially substituted for Sr is completely suppressed for the Sr free sample $Hg_{0.09}Ca_2Co_{2.51}$, the room temperature resistivity being the smallest for this compound. At the present time, there exists only one quantitative and single model to correlate the S variation to the oxidation state of the cobalt species lying in the $[CoO_2]$ conducting layer [16]. This model, based on the generalized Heikes formula, leads to the following expression:

$$S = -86.2 \ln\left[\frac{1}{6}\frac{1}{1-x}\right](\mu V\,K^{-1}),$$

where x is the fraction of holes, $x = Co^{4+}/Co$, sitting on the cobalt sites.

By using this formula with the S values found for the pure Sr and Ca mercury-based cobaltites, $S_{300\,K} = +115\,\mu V\,K^{-1}$ and $S_{300\,K} = +130\,\mu V\,K^{-1}$, the average Co oxidation state values are obtained, $V_{Co} = 3.61$ and $V_{Co} = 3.57$, respectively. This demonstrates that only a small change of the cobalt mixed valence can be responsible for a significant S increase. This shows also that a decrease of the formal valence of cobalt in the $[CoO_2]$ layer is beneficial to the thermopower.

4. Conclusion

Introducing Hg cations in the form of a mixed $[(Hg,Co)O]^{RS}$ layer sandwiched between two $[SrO]^{RS}$ has allowed us to prepare a new series of the misfit cobaltites $[Hg_{1-x}Co_xSr_{2-y}Ca_yO_3]^{RS}[CoO_2]_{b1/b2}$ characterized by the intergrowth of three rock salt-type layers with one CdI_2-type $[CoO_2]$ layer. Furthemore, the complete substitution of Ca for Sr in the cobaltite is found to affect significantly the mismatch b_1/b_2 between the two sublattices. Compared to the Tl- and Pb-based isostructural cobaltites, the Hg content cannot exceed 40% of the middle rock salt-type layer whereas it can

reach 70% and 100% for Pb- and Tl-misfit cobaltites, respectively. This outlines the mixed nature of the mercury-based layer that was previously found in the superconducting cuprates. These new cobaltites exhibit large thermopower values at room temperature together with low resistivity values. These compounds would certainly deserve further measurements at higher temperatures to check their stability in air and measure their figure of merit.

References

[1] I. Terasaki, Y. Sasago, K. Uchinokura, Phys. Rev. B 56 (1997) R12685.
[2] S. Li, R. Funahashi, I. Matsubara, K. Ueno, Y. Yamada, J. Mater. Chem. 9 (1999) 1659.
[3] A.C. Masset, C. Michel, A. Maignan, M. Hervieu, O. Toulemonde, F. Studer, B. Raveau, J. Hejtmanek, Phys. Rev. B 62 (2000) 166.
[4] Y. Miyazaki, M. Onoda, T. Oku, M. Kikuchi, Y. Ishii, Y. Ono, Y. Morii, T. Kajitani, J. Phys. Soc. Jpn. 71 (2002) 491.
[5] I. Matsubara, R. Funahashi, T. Takenchi, S. Sadeoka, T. Shimizu, K. Heno, Appl. Phys. Lett. 78 (2001) 3627.
[6] S. Lambert, H. Leligny, D. Grebille, J. Solid State Chem. 160 (2001) 322–331.
[7] D.J. Singh, Phys. Rev. B 61 (2000) 13397.
[8] Ph. Boullay, R. Seshadri, F. Studer, M. Hervieu, D. Groult, B. Raveau, Chem. Mater. 10 (1998) 92; Ph. Boullay, Thesis, University of Caen, 1997.
[9] A. Maignan, L.B. Wang, S. Hébert, D. Pelloquin, B. Raveau, Chem. Mater 14 (3) (2002) 1231–1235.
[10] D. Pelloquin, A. Maignan, S. Hébert, C. Martin, M. Hervieu, C. Michel, L.B. Wang, B. Raveau, Chem. Mater 14 (7) (2002) 3100–3105.
[11] A. Maignan, D. Pelloquin, S. Hébert, C. Michel, J. Hejtmanek, J. Appl. Phys. 92 (2002) 1964.
[12] O. Chmaissen, D.N. Argyriou, D.G. Hinks, J.D. Jorgensen, B.G. Storey, H. Zhang, L.D. Marks, Y.Y. Wang, V.P. Dravid, B. Dabrowski, Phys. Rev B 52 (1995) 15636;
S. Malo, C. Michel, D. Pelloquin, M. Hervieu, O. Toulemonde, B. Raveau, Physica C 304 (1998) 213.
[13] V. Petricek, et al., JANA 2000 software, Institute of Physics Academy of Science of the Czech Republik, Prague.
[14] A. Maignan, D. Pelloquin, C. Martin, M. Hervieu, B. Raveau, J. Mater. Chem. 12 (4) (2002) 1009–1016.
[15] A.C. Masset, O. Toulemonde, D. Pelloquin, E. Suard, A. Maignan, F. Studer, M. Hervieu, C. Michel, Int. J. Inorg. Mater. 2 (2000) 687–699.
[16] W. Koshibae, K. Tsutsui, S. Maekawa, Phys. Rev. B 62 (2000) 68697.